Rounding corners of nano-square patches for multispectral plasmonic metamaterial absorbers

Sencer Ayas,[1,*] Gokhan Bakan,[1] and Aykutlu Dana[1,2]

[1] *UNAM Institute of Materials Science and Nanotechnology, Bilkent University, 06800 Ankara, Turkey*
[2] *aykutlu@unam.bilkent.edu.tr*
[*]ayas@unam.bilkent.edu.tr

Abstract: Multispectral metamaterial absorbers based on metal-insulator-metal nano-square patch resonators are studied here. For a geometry consisting of perfectly nano-square patches and vertical sidewalls, double resonances in the visible regime are observed due to simultaneous excitation of electric and magnetic plasmon modes. Although slightly modifying the sizes of the square patches makes the resonance wavelengths simply shift, rounding corners of the square patches results in emergence of a third resonance due to excitation of the circular cavity modes. Sidewall angle of the patches are also observed to affect the absorption spectra significantly. Peak absorption values for the triple resonance structures are strongly affected as the sidewall angle varies from 90 to 50 degrees. Rounded corners and slanted sidewalls are typical imperfections for lithographically fabricated metamaterial structures. The presented results suggest that imperfections caused during fabrication of the top nano-structures must be taken into account when designing metamaterial absorbers. Furthermore, it is shown that these fabrication imperfections can be exploited for improving resonance properties and bandwidths of metamaterials for various potential applications such as solar energy harvesting, thermal emitters, surface enhanced spectroscopies and photodetection.

References and links

1. T. V. Teperik, F. J. García de Abajo, G. Borisov, M. Abdelsalam, P. N. Bartlett, Y. Sugawara, and J. J. Baumberg, "Omnidirectional absorption in nanostructured metal surfaces," Nat. Photonics **2**(5), 299–301 (2008).
2. J. Valentine, S. Zhang, T. Zentgraf, E. Ulin-Avila, D. A. Genov, G. Bartal, and X. Zhang, "Three-dimensional optical metamaterial with a negative refractive index," Nature **455**(7211), 376–379 (2008).
3. E. Cubukcu, S. Zhang, Y.-S. Park, G. Bartal, and X. Zhang, "Split ring resonator sensors for infrared detection of single molecular monolayers," Appl. Phys. Lett. **95**(4), 043113 (2009).
4. C. Cao, J. Zhang, X. Wen, S. L. Dodson, N. T. Dao, L. M. Wong, S. Wang, S. Li, A. T. Phan, and Q. Xiong, "Metamaterials-based label-free nanosensor for conformation and affinity biosensing," ACS Nano **7**(9), 7583–7591 (2013).
5. M. W. Knight, H. Sobhani, P. Nordlander, and N. J. Halas, "Photodetection with active optical antennas," Science **332**(6030), 702–704 (2011).
6. F. Yi, H. Zhu, J. C. Reed, and E. Cubukcu, "Plasmonically enhanced thermomechanical detection of infrared radiation," Nano Lett. **13**(4), 1638–1643 (2013).
7. F. Yi, H. Zhu, J. C. Reed, A. Y. Zhu, and E. Cubukcu, "Thermoplasmonic membrane-based infrared detector," IEEE Photon. Technol. Lett. **26**(2), 202–205 (2014).
8. F. B. P. Niesler, J. K. Gansel, S. Fischbach, and M. Wegener, "Metamaterial metal-based bolometers," Appl. Phys. Lett. **100**(20), 203508 (2012).
9. V. Savinov, V. A. Fedotov, P. A. J. de Groot, and N. I. Zheludev, "Radiation-harvesting resonant superconducting sub-THz metamaterial bolometer," Supercond. Sci. Technol. **26**(8), 084001 (2013).
10. N. I. Landy, S. Sajuyigbe, J. J. Mock, D. R. Smith, and W. J. Padilla, "Perfect metamaterial absorber," Phys. Rev. Lett. **100**(20), 207402 (2008).
11. J. W. Park, P. V. Tuong, J. Y. Rhee, K. W. Kim, W. H. Jang, E. H. Choi, L. Y. Chen, and Y. Lee, "Multi-band metamaterial absorber based on the arrangement of donut-type resonators," Opt. Express **21**(8), 9691–9702 (2013).

12. H. Wakatsuchi, S. Greedy, C. Christopoulos, and J. Paul, "Customised broadband metamaterial absorbers for arbitrary polarisation," Opt. Express **18**(21), 22187–22198 (2010).
13. M. Diem, T. Koschny, and C. Soukoulis, "Wide-angle perfect absorber/thermal emitter in the terahertz regime," Phys. Rev. B **79**(3), 033101 (2009).
14. H. Tao, N. I. Landy, C. M. Bingham, X. Zhang, R. D. Averitt, and W. J. Padilla, "A metamaterial absorber for the terahertz regime: Design, fabrication and characterization," Opt. Express **16**(10), 7181–7188 (2008).
15. R. Alaee, C. Menzel, C. Rockstuhl, and F. Lederer, "Perfect absorbers on curved surfaces and their potential applications," Opt. Express **20**(16), 18370–18376 (2012).
16. J. Hao, J. Wang, X. Liu, W. J. Padilla, L. Zhou, and M. Qiu, "High performance optical absorber based on a plasmonic metamaterial," Appl. Phys. Lett. **96**(25), 251104 (2010).
17. J. Hao, L. Zhou, and M. Qiu, "Nearly total absorption of light and heat generation by plasmonic metamaterials," Phys. Rev. B **83**(16), 165107 (2011).
18. N. Liu, M. Mesch, T. Weiss, M. Hentschel, and H. Giessen, "Infrared perfect absorber and its application as plasmonic sensor," Nano Lett. **10**(7), 2342–2348 (2010).
19. X. Liu, T. Tyler, T. Starr, A. F. Starr, N. M. Jokerst, and W. J. Padilla, "Taming the blackbody with infrared metamaterials as selective thermal emitters," Phys. Rev. Lett. **107**(4), 045901 (2011).
20. X. Liu, T. Starr, A. F. Starr, and W. J. Padilla, "Infrared spatial and frequency selective metamaterial with near-unity absorbance," Phys. Rev. Lett. **104**(20), 207403 (2010).
21. M. Pu, C. Hu, M. Wang, C. Huang, Z. Zhao, C. Wang, Q. Feng, and X. Luo, "Design principles for infrared wide-angle perfect absorber based on plasmonic structure," Opt. Express **19**(18), 17413–17420 (2011).
22. J. Wang, Y. Chen, X. Chen, J. Hao, M. Yan, and M. Qiu, "Photothermal reshaping of gold nanoparticles in a plasmonic absorber," Opt. Express **19**(15), 14726–14734 (2011).
23. L. P. Wang and Z. M. Zhang, "Wavelength-selective and diffuse emitter enhanced by magnetic polaritons for thermophotovoltaics," Appl. Phys. Lett. **100**(6), 063902 (2012).
24. R. Alaee, C. Menzel, U. Huebner, E. Pshenay-Severin, S. Bin Hasan, T. Pertsch, C. Rockstuhl, and F. Lederer, "Deep-subwavelength plasmonic nanoresonators exploiting extreme coupling," Nano Lett. **13**(8), 3482–3486 (2013).
25. K. Aydin, V. E. Ferry, R. M. Briggs, and H. A. Atwater, "Broadband polarization-independent resonant light absorption using ultrathin plasmonic super absorbers," Nat Commun **2**, 517 (2011).
26. J. A. Bossard, L. Lin, S. Yun, L. Liu, D. H. Werner, and T. S. Mayer, "Near-ideal optical metamaterial absorbers with super-octave bandwidth," ACS Nano **8**(2), 1517–1524 (2014).
27. M. G. Nielsen, A. Pors, O. Albrektsen, and S. I. Bozhevolnyi, "Efficient absorption of visible radiation by gap plasmon resonators," Opt. Express **20**(12), 13311–13319 (2012).
28. J. Wang, C. Fan, P. Ding, J. He, Y. Cheng, W. Hu, G. Cai, E. Liang, and Q. Xue, "Tunable broad-band perfect absorber by exciting of multiple plasmon resonances at optical frequency," Opt. Express **20**(14), 14871–14878 (2012).
29. X. Wang, C. Luo, G. Hong, and X. Zhao, "Metamaterial optical refractive index sensor detected by the naked eye," Appl. Phys. Lett. **102**(9), 091902 (2013).
30. P. Zhu and L. Jay Guo, "High performance broadband absorber in the visible band by engineered dispersion and geometry of a metal-dielectric-metal stack," Appl. Phys. Lett. **101**(24), 241116 (2012).
31. M. Elbahri, M. K. Hedayati, V. S. Kiran Chakravadhanula, M. Jamali, T. Strunkus, V. Zaporojtchenko, and F. Faupel, "An omnidirectional transparent conducting-metal-based plasmonic nanocomposite," Adv. Mater. **23**(17), 1993–1997 (2011).
32. M. K. Hedayati, M. Javaherirahim, B. Mozooni, R. Abdelaziz, A. Tavassolizadeh, V. S. Chakravadhanula, V. S. K. Zaporojtchenko, T. Strunkus, F. Faupel, and M. Elbahri, "Design of a perfect black absorber at visible frequencies using plasmonic metamaterials," Adv. Mater. **23**(45), 5410–5414 (2011).
33. A. Moreau, C. Ciracì, J. J. Mock, R. T. Hill, Q. Wang, B. J. Wiley, A. Chilkoti, and D. R. Smith, "Controlled-reflectance surfaces with film-coupled colloidal nanoantennas," Nature **492**(7427), 86–89 (2012).
34. Y. Cui, K. H. Fung, J. Xu, H. Ma, Y. Jin, S. He, and N. X. Fang, "Ultrabroadband light absorption by a sawtooth anisotropic metamaterial slab," Nano Lett. **12**(3), 1443–1447 (2012).
35. Z. H. Jiang, S. Yun, F. Toor, D. H. Werner, and T. S. Mayer, "Conformal dual-band near-perfectly absorbing mid-infrared metamaterial coating," ACS Nano **5**(6), 4641–4647 (2011).
36. C. D'Andrea, J. Bochterle, A. Toma, C. Huck, F. Neubrech, E. Messina, B. Fazio, O. M. Maragò, E. Di Fabrizio, M. Lamy de La Chapelle, P. G. Gucciardi, and A. Pucci, "Optical nanoantennas for multiband surface-enhanced infrared and Raman spectroscopy," ACS Nano **7**(4), 3522–3531 (2013).
37. B. Zhang, Y. Zhao, Q. Hao, B. Kiraly, I.-C. Khoo, S. Chen, and T. J. Huang, "Polarization-independent dual-band infrared perfect absorber based on a metal-dielectric-metal elliptical nanodisk array," Opt. Express **19**(16), 15221–15228 (2011).
38. C.-W. Cheng, M. N. Abbas, C.-W. Chiu, K.-T. Lai, M.-H. Shih, and Y.-C. Chang, "Wide-angle polarization independent infrared broadband absorbers based on metallic multi-sized disk arrays," Opt. Express **20**(9), 10376–10381 (2012).
39. J. Hendrickson, J. Guo, B. Zhang, W. Buchwald, and R. Soref, "Wideband perfect light absorber at midwave infrared using multiplexed metal structures," Opt. Lett. **37**(3), 371–373 (2012).
40. E. Lansey, I. R. Hooper, J. N. Gollub, A. P. Hibbins, and D. T. Crouse, "Light localization, photon sorting, and enhanced absorption in subwavelength cavity arrays," Opt. Express **20**(22), 24226–24236 (2012).
41. J. Le Perchec, Y. Desieres, N. Rochat, and R. Espiau de Lamaestre, "Subwavelength optical absorber with an integrated photon sorter," Appl. Phys. Lett. **100**(11), 113305 (2012).

42. W. Ma, Y. Wen, and X. Yu, "Broadband metamaterial absorber at mid-infrared using multiplexed cross resonators," Opt. Express **21**(25), 30724–30730 (2013).
43. H. Ko, D.-H. Ko, Y. Cho, and I. K. Han, "Broadband light absorption using a multilayered gap surface plasmon resonator," Appl. Phys., A Mater. Sci. Process. **116**(3), 857–861 (2014).
44. P. Pitchappa, C. P. Ho, P. Kropelnicki, N. Singh, D.-L. Kwong, and C. Lee, "Dual band complementary metamaterial absorber in near infrared region," J. Appl. Phys. **115**(19), 193109 (2014).
45. S. Ayas, H. Güner, B. Türker, O. O. Ekiz, F. Dirisaglik, A. K. Okyay, and A. Dâna, "Raman enhancement on a broadband meta-surface," ACS Nano **6**(8), 6852–6861 (2012).
46. D. Li, L. Qin, X. Xiong, R.-W. Peng, Q. Hu, G.-B. Ma, H.-S. Zhou, and M. Wang, "Exchange of electric and magnetic resonances in multilayered metal/dielectric nanoplates," Opt. Express **19**(23), 22942–22949 (2011).
47. C. Koechlin, P. Bouchon, F. Pardo, J. L. Pelouard, and R. Haïdar, "Analytical description of subwavelength plasmonic MIM resonators and of their combination," Opt. Express **21**(6), 7025–7032 (2013).
48. R. Filter, J. Qi, C. Rockstuhl, and F. Lederer, "Circular optical nanoantennas: an analytical theory," Phys. Rev. B **85**(12), 125429 (2012).
49. F. Minkowski, F. Wang, A. Chakrabarty, and Q.-H. Wei, "Resonant cavity modes of circular plasmonic patch nanoantennas," Appl. Phys. Lett. **104**(2), 021111 (2014).
50. Y. Chu, M. G. Banaee, and K. B. Crozier, "Double-resonance plasmon substrates for surface-enhanced Raman scattering with enhancement at excitation and stokes frequencies," ACS Nano **4**(5), 2804–2810 (2010).

1. Introduction

Perfect absorption of light can be achieved by exciting surface plasmons on textured metallic surfaces [1]. Metamaterials (MMs) are known as nanostructured metal surfaces to tailor the optical properties. So far, MMs are used for designing negative index materials [2], optical sensor platforms [3], surface enhanced Raman spectroscopy substrate [4], solar cells [5], thermoplasmonic detectors [6,7] and optical bolometer imaging systems [8,9]. Metamaterial absorbers (MMAs) are arrays of patterned metal-insulator-metal (MIM) structures that have almost perfect absorption for certain wavelengths where their impedances are perfectly matched to that of air near the resonant wavelengths. Nearly perfect MMAs are demonstrated in the microwave [10–12], terahertz [13,14], infrared (IR) [15–23] and visible regimes [24–30]. Metamaterial absorbers in the visible spectrum can be realized using nanoparticles on a thick metallic ground plane separated with a dielectric spacer [31–33]. Typically, MMAs have narrow bands or single resonances attributed to their identical resonators in every unit cell [25,26,34,35]. On the other hand, multispectral characteristic of a metamaterial plasmonic surface has a great potential for various applications such as infrared absorption spectroscopy and surface enhanced Raman spectroscopy where presence of the resonances are generally accompanied by high field enhancements [36]. Recently, broadband or multispectral MMAs are demonstrated in the visible and IR wavelengths using more complex geometries. Multiplexing different resonator structures in a unit cell is a route to obtain multispectral absorption which requires precise control of dimensions of multiple nanostructures [11, 37–43]. Multispectral MMAs based on simultaneous excitation of electric and magnetic plasmon modes are the least exploited structures [28,44,45]. MMAs are usually fabricated by using electron beam (e-beam) or optical lithography which typically result in structures slightly different from the design. For example, disc structures with straight sidewalls come out as truncated cones with slanted sidewalls and square structures acquire rounded corners during lithography. These imperfections are exploited using a MMA structure which has multispectral absorbance bands due to excitation of both electric and magnetic plasmon modes. Specifically, when corners of the top nano-square patches are rounded, a new resonance emerges. The provided analysis is expected to be more realistic as it accounts for imperfections caused by common fabrication techniques. The studied MMA structure only requires accurate control of top nano-square patch widths to obtain a multispectral and broadband response, unlike more complex multiplexed metamaterial structures with multiple resonators with different geometries in a unit cell.
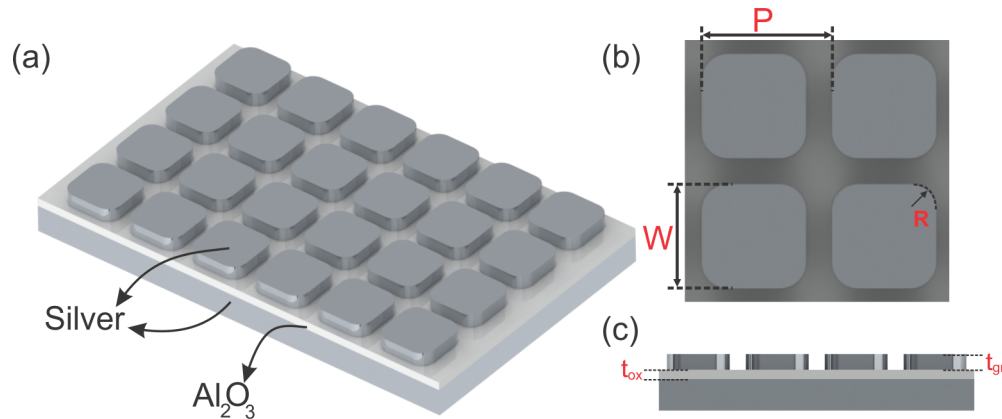
Fig. 1. 3D illustration of the studied MMA surface (a). Top (b) and side (c) views. Periods in x and y directions are 250nm. W is the nano-square width and R is the curvature of the corners.

2. Results and discussion

The studied structure is based on a metal/insulator/nano-square array geometry [Fig. 1]. Silver is used for both bottom metallic plane and top nano-square arrays. Alumina (Al_2O_3) is used as the dielectric spacer layer. 100nm thick bottom (ground) plane is used for all the simulations where transmission is almost zero in the visible regime. Thickness of the top layer is chosen as 50nm, allowing coupling of localized surface plasmon modes due to interactions between adjacent square patches. Periods of the square patches along x, y directions are 250nm. The simulations are based on the Finite Difference Time Domain (FDTD) method. Material properties (complex and real parts of dielectric functions) for silver and alumina are obtained from the program's material database and fitted to a 12th order polynomial function (Palik data). Mesh size used in the finite element analysis is 2nm in both x and y directions and 1nm in z direction. Broadband electromagnetic plane wave is used for the normal incidence illumination with 400nm-750nm wavelength range. Bloch boundary conditions are chosen for x and y directions and a perfectly matched layer (PML) is used along z direction. Simulation durations are further reduced by using asymmetric and symmetric boundary conditions along x and y directions, respectively.

Figure 2(a) shows absorption spectra for the perfect square patches (R = 0nm). When there is no oxide in the structures, a single resonance at λ = 530nm is observed due to the cavity resonance between the patches (in the grooves). When, an oxide spacer (t_{ox} = 30nm of) is included, the resonance splits into 2 modes at λ_1 = 480nm and λ_2 = 605nm as shown in Fig. 2(a). To understand the origin of these resonances electric and magnetic field distributions are investigated as shown in Figs. 2(c) and 2(d). Without the oxide layer, magnetic field is localized in the grooves and electric field is higher at the top of the adjacent ridges. This resonance resembles an electric plasmon mode. With the oxide layer, magnetic field is also confined in the grooves at λ_1 = 480nm. For λ_2 = 605nm, magnetic field is confined in the spacer layer (the 3rd order mode, the fundamental mode is observed in the NIR regime). Hence, resonances at λ_1 = 480nm and λ_2 = 605nm are electric and magnetic plasmon modes, respectively. The small peak around 550nm is due to a higher order magnetic plasmon mode (m = 5). As nano-square patch corners are rounded, the symmetry conditions causing the excitation of these higher order magnetic plasmon modes change which result in disappearance of the 5th order magnetic plasmon mode around λ = 550nm. Then, we investigate the effect of the nano-square patch width (W) as shown in Fig. 2(b). The resonance at shorter wavelength is unaffected with increasing W which also suggests that this resonance is an electric plasmon mode [28,46]. However, as the width increases the resonance at higher wavelength shows a redshift which verifies that this is a magnetic plasmon mode. This resonance can be explained in terms of standing waves and can be expressed as λ_r =

$2n_{eff}W + \theta$, where n_{eff} is the effective refractive index of the MIM mode, θ is the phase term due to reflections from the edges. The resonance wavelength and W show a linear relationship [47].
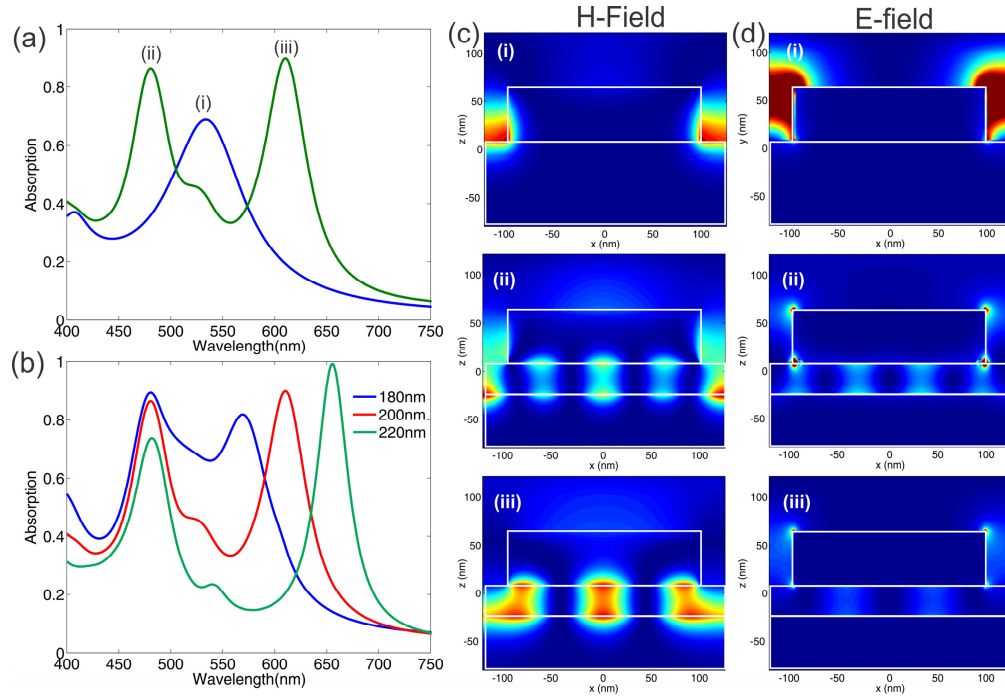

Fig. 2. Absorption spectra for perfect nano-square patches (R = 0nm, straight sidewalls) for t_{ox} = 0 (blue) and t_{ox} = 30nm (green) (a). Absorption spectra for various nano-square patch widths (t_{ox} = 30 nm) (b). Magnetic (c) and electric (d) field profiles at the resonances shown in (a).

When the structures are fabricated using electron beam lithography, due to the finite point-spread function width of the electron beam, the corners acquire a finite curvature. Hence, the corners of the nano-square patches are rounded in the simulations (See Fig. 1). Figure 3 shows emergence of a third mode whose resonance frequency is affected by radius of the corners (R). For W = 200nm and R between 0 nm and 40nm there are two distinct resonances as shown in Figs. 3(a) and 3(b). When the curvature is further increased, the magnetic plasmon mode splits into two. For R = 100nm the nano-square patches become perfect discs and three resonances are observed with almost equal wavelength spacing. The absorption of each resonance is higher than 85%. When W is increased slightly (W = 210nm) splitting of the magnetic plasmon mode is observed at a smaller curvature value (R~30nm). The wavelength spacing between the resonances is the highest for the maximum curvature value (R = 105nm for W = 210 nm) and near perfect absorption is seen for the middle resonance around 550-600 nm [Figs. 3(c) and 3(d)]. We further investigate the effect of oxide thickness on the absorption of the triple band plasmonic structures as shown in Figs. 3(e) and 3(f). The electric plasmon mode at λ~500nm is almost independent of the spacer thickness as expected. However, the magnetic plasmon modes strongly depend on the spacer thickness due to varying effective refractive index of the MIM waveguide formed by the top patches and bottom Ag layer with increasing spacer thickness.
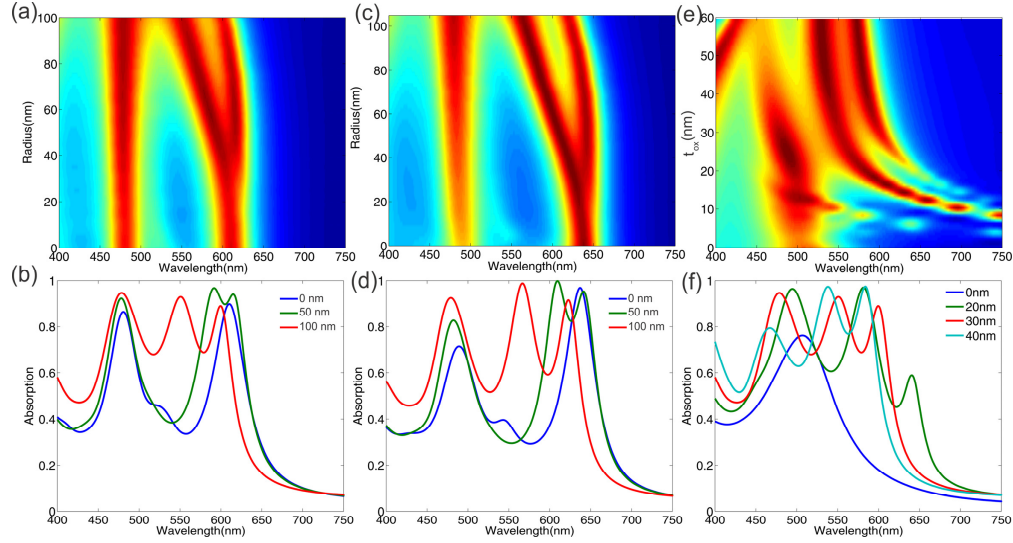
Fig. 3. Absorption spectra for varying curvature radius for W = 200nm (a), (b) and W = 210nm (c), (d) with t$_{ox}$ = 30nm. Absorption spectra for varying oxide thickness for W = 200nm and R = 100nm (e), (f).

In order to understand the origins of the resonances for the perfect top nano-discs layer (R = 100nm, W = 200nm), we study the electric field profiles at λ = 550nm and λ = 600nm. The analytical approaches for circular nano patch antennas have been recently demonstrated [48,49]. Following the steps reported in the previous literature, the Helmholtz equation for metal-insulator-metal geometry is solved in the cylindrical coordinates using:

$$\frac{\partial}{\partial \rho}(\rho \frac{\partial E_z}{\partial \rho}) + \frac{1}{\rho^2}(\rho \frac{\partial^2 E_z}{\partial \varphi^2}) + \frac{\partial^2 E_z}{\partial z^2} + k^2 E_z = 0 \qquad (1)$$

The solution to [Eq. (1)] is given by $E_z = J_m(k_{sp}\rho)\cos(m\varphi + \vartheta)(Ae^{k_z z} + Be^{-k_z z})$ with Neumann boundary condition $\partial E_z / \partial \rho = 0$, where k_{sp} is the wave-vector for the MIM cavity. The solution to electric field distribution is given in terms of even and odd modes expressed as E(O)$_{mn}$ where n is the order of the roots for $\partial(J_m(k_{sp}\rho))/\partial \rho = 0$. For odd and even values of m odd and even order modes are excited, respectively. The simulated and calculated mode profiles are shown in Fig. 4. For λ = 550nm which emerges when corners are rounded, O$_{12}$ mode is excited as shown in Figs. 4(a) and 4(c) while the magnetic plasmon mode at λ = 600nm resembles O$_{31}$ mode [Figs. 4(b) and 4(d)].
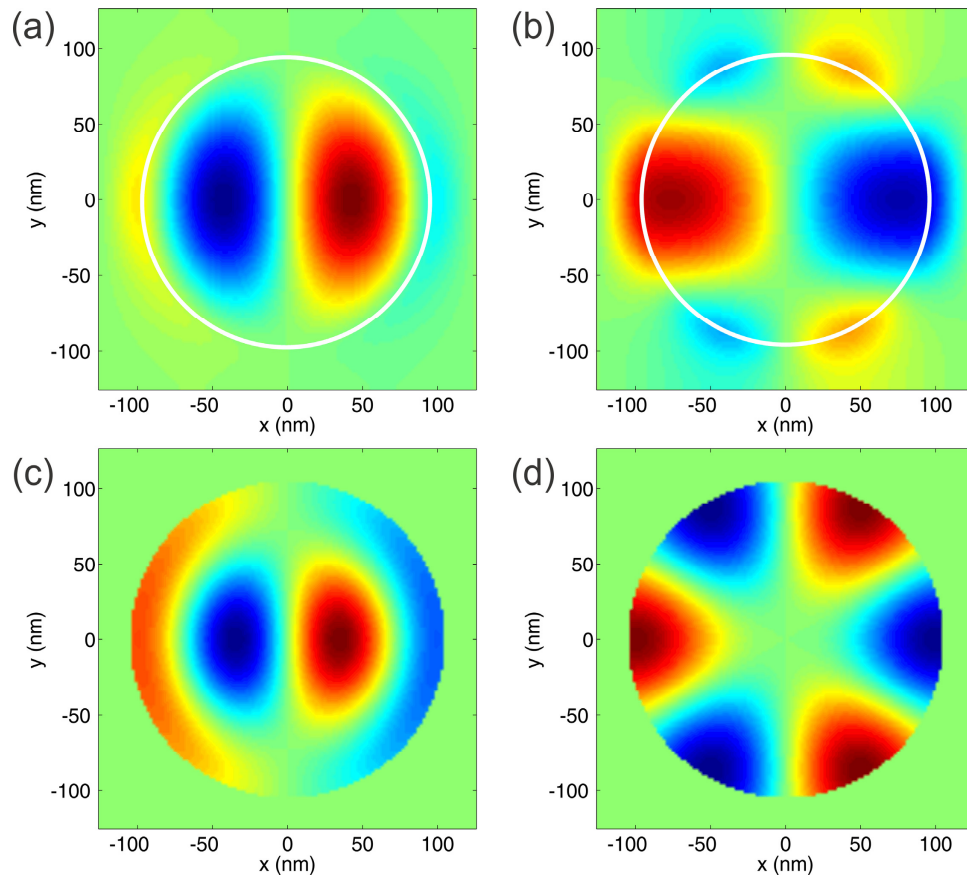
Fig. 4. Origin of resonances for W = 200nm, R = 100nm and t_{ox} = 30nm. Simulated z component of electric field profiles for λ = 550nm (a) and λ = 600nm (b). Calculated electrical field profiles for modes m = 1, n = 2 (c) and m = 3, n = 1 (d).

Fabrication of MMAs requires lithography and liftoff processes which results in slanted sidewalls of patterned surfaces. Figure 5(a) shows cross section of a typical MMA structure. To demonstrate the effect of the sidewall angle on the absorption spectra, we study truncated cones as the top metallic layer with varying sidewall angle. Absorption spectra of such structures are shown in Figs. 5(b) and 5(c). As the sidewall angle decreases down to θ = 75 degrees a resonance at λ = 600nm can be observed. While this resonance disappears for smaller sidewall angles, a broad absorption band ranging from 400 to 550nm is observed. For θ = 85 degrees or higher, a triple band absorption is observed. Such a structure with high sidewall angles can be fabricated using inductively coupled plasma or reactive ion etching, after e-beam lithography on MIM films.
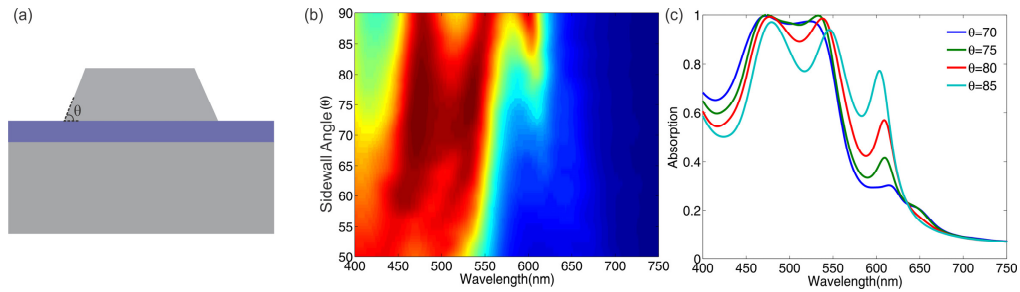
Fig. 5. Cross section of the simulated structure (a). Absorption spectra for varying sidewall angle for W = 200nm, R = 100nm (b), (c).

3. Conclusions

In conclusion, we present a metamaterial absorber structure using simultaneous excitation of electric and magnetic plasmon modes. We investigate the effect of lithography related imperfections in nano structures such as the effect of corner rounding on MIM structures, which shows triple band absorption due to excitation of circular cavity modes confirmed by solving the Helmholtz equation in cylindrical coordinates. The studied structures account for fabrication imperfections which can be exploited to obtain the desired spectral response by tuning the top layer properties such as the nano-square patch width and curvature. Slanted sidewalls of the top nanodiscs are also observed to affect the absorption spectra. Such structures with multiple resonances in the visible regime can be useful for Surface Enhanced Raman Spectroscopy (SERS) which relies on enhanced Raman signal with excitation of multiple plasmon modes [50]. This study can help design of novel thermal emitter devices using the same principles in the IR wavelengths, plasmon enhanced photodetection and solar energy conversion devices.

Acknowledgments